An Ultrawide-Bandwidth Tapered Resistive TEM Horn Antenna

Li-Chung T. Chang and Walter D. Burnside, *Fellow, IEEE*

***Abstract*—A novel stable beamwidth, ultrawide-bandwidth low-scattering antenna is presented in this paper. This antenna is a modified version of the conducting slotline bowtie hybrid (SBH) antenna with resistive sheets (Rcards) introduced into the guiding structure design. Since the resistive sheets can attenuate creeping wave fields, much smaller rolled edges are needed in the Rcard SBH antenna. Moreover, due to the Rcard's partially transparent nature with respect to electromagnetic fields, the radar cross section (RCS) associated with this new antenna is smaller than the original conducting rolled edge one. By employing an optimization process based on the concept of the genetic algorithm, one can easily design the Rcard SBH antenna to obtain a very stable antenna beamwidth and phase center in both the E- and H-planes across the entire operating frequency bandwidth. Because of its constant beamwidth, low RCS, and broad-band features, the Rcard SBH antenna is an ideal antenna for many applications such as a compact range feed. Calculated and measured results are presented to demonstrate the performance of this new antenna.**

***Index Terms*—Rcard, tapered, TEM horn antenna, ultrawide-band.**

I. Introduction

A COMMON feature associated with a traditional broad-band horn antenna is that its beamwidth is strongly dependent on the operating frequency. In fact, for most wide-band horn antennas such as the AEL horn (model H-1498) [1] and quadridged circular horn (Model A6200) [2], the 3-dB beamwidth decreases as the operating frequency increases. This is not desirable for applications that require uniform illumination covering a certain angular sector around the mainbeam area. For example, a compact range feed is required to possess constant beamwidth with a well-defined plateau mainbeam to reduce the taper error.

The conducting rolled-edge slotline bowtie hybrid (SBH) antenna [3] was one of the first linearly polarized antennas to possess these features. This antenna was constructed by integrating two main structures, namely, a tapered slotline and a bowtie TEM horn. To improve its voltage standing-wave ratio (VSWR), a microstrip-slotline Y–Y transition [4] was used as the ultrawide-band feeding structure. A Vivaldi taper transition [5] and rolled-edge [6] termination were then employed to provide better impedance transitions between the throat section and aperture, respectively. It was found that the edge waves existing on the bowtie guiding structure degraded the radiation performance; therefore, proper absorber treatment is normally required to achieve the best performance.

This type of SBH antenna has been successfully used in ultrawide-bandwidth applications for many years [7], [8]; however, its large geometry (conducting rolled-edge structure) affects its scattering performance, which limits its potential applications. In this paper, an Rcard version of the SBH antenna is introduced. This novel antenna is fabricated by integrating resistive sheets (Rcards) into a blended rolled-edge geometry to terminate the SBH structure. To provide a good impedance match to free space, the Rcards are designed with an appropriate tapered resistive profile. Since resistive sheets can attenuate surface fields [9], much smaller rolled edges are needed such that this new antenna basically performs the same as the original conducting SBH antenna [3]. The major improvement is the smaller antenna radar cross section (RCS) due to the employment of the resistive sheets as opposed to the large rolled edges.

The rest of this paper is organized as follows. In Section II, the feeding structure of the Rcard SBH antenna is discussed. Basically, the same feeding structure used in the conducting SBH antenna is employed here due to its excellent broad-band performance. In Section III, the antenna guiding structure is analyzed. Due to the employment of the Rcard materials in the guiding structure, more design parameters must be considered. To accomplish this task, the relationships between the radiation pattern and the design parameters are investigated based on numerical analysis techniques. Due to the open structure of the SBH antenna, proper absorber treatment is required to achieve the desired performance, which will be discussed in Section IV. In Section V, two design examples of the Rcard SBH antenna are presented and their performance verified by comparison with measured results. Also, an optimization process based on the genetic algorithm (GA) concept [10] is discussed to properly design the antenna. Finally, a summary and some general conclusions are given in Section VI.

II. Feeding Structure Overview of the SBH Antenna

The feeding structure consists of a microstrip to slotline Y–Y transition balun is shown in Fig. 1. The microstrip "Y" and the slotline "Y" are located on the opposite sides of a substrate and face each other. The one arm of the "Y" is terminated in a short circuit and the other in an open circuit, which means that the reflected waves from the two ends of the "Y" geometry tend to cancel each other when they reunite at the junction [7], [11]. In general, the bandwidth of this feeding structure is limited by

Manuscript received January 13, 1997; revised November 16, 2000. This work was supported by Rockwell International Corporation under Contract T2X2-DM-601448 with The Ohio State University Research Foundation.

L.-C. T. Chang is with Lucent Technologies, Whippany, NJ 07981 USA.

W. D. Burnside is with the ElectroScience Laboratory, The Ohio State University, Columbus, OH 43212 USA.

Publisher Item Identifier S 0018-926X(00)10863-4.

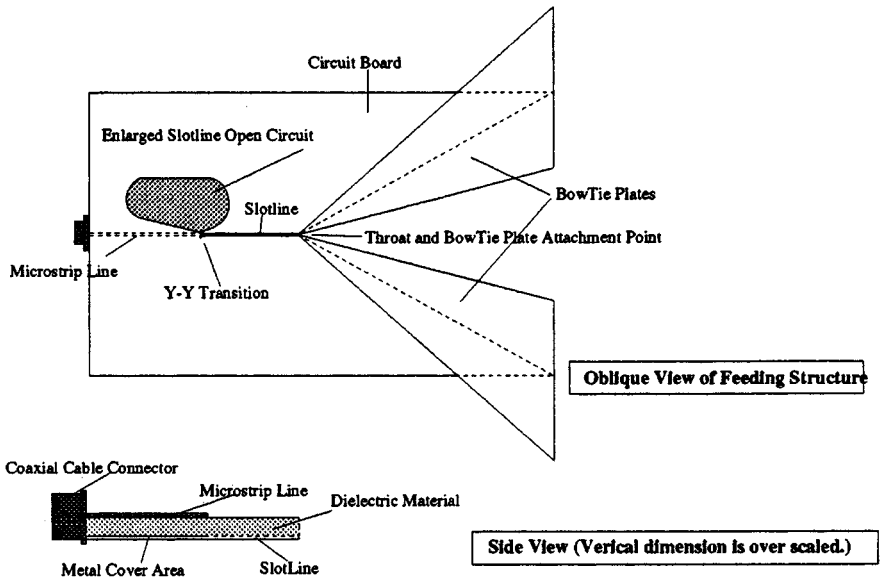

Fig. 1. Y–Y microstrip/slotline balun feeding structure.

the size of the slotline open circuit. A very good transmission coefficient (S_{21}) can be obtained over a very broad bandwidth (444 : 1) by using a reasonable circuit board size [3]. The small reflection and nearly perfect transmission clearly indicate that the Y–Y junction radiation loss is very small.

III. Antenna Guiding Structure Analysis

Due to its broad-band feature, the bowtie TEM horn is chosen as the guiding structure for the SBH antenna. In order to improve the impedance transition from the slotline to free space, the bowtie guiding structure has a smoothly curved shape that consists of Vivaldi, linear, and rolled-edge sections, as shown in Fig. 2. The governing functions associated with each of these three sections are listed below.

1) Vivaldi Section:

$$y - y_a = e^{A(x-x_a)} - A(x - x_a) - 1, \quad \text{for } x_a \le x \le x_b \tag{1}$$

where A is the exponential factor and is given by

$$A = \tan(\theta/2)/(e^{A(x_b - xa)} - 1) \tag{2}$$

and θ is the flare angle.

2) Linear Section:

$$y - y_b = \tan(\theta/2)(x - x_b), \qquad \text{for } x_b \le x \le x_c. \tag{3}$$

3) Blended Rolled Edge Section:

$$x = x_e + b_e \sin\left(\frac{\theta}{2}\right)(1.0 - \cos(\alpha))\, f(\alpha) \tag{4}$$

$$y = y_e - b_e \cos\left(\frac{\theta}{2}\right)(1.0 - \cos(\alpha))\, f(\alpha) \tag{5}$$

where, if linear blending

$$f(\alpha) = 1.0 - \frac{\alpha}{\alpha_s} \tag{6}$$

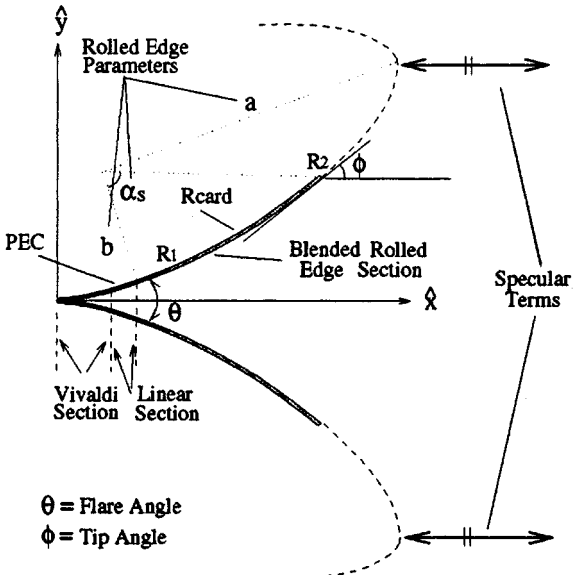

Fig. 2. Guiding structure geometry for new Rcard SBH antenna.

or, if cosine blending

$$f(\alpha) = \cos\left(\frac{\pi\alpha}{2\alpha_s}\right) \tag{7}$$

and

$$x_e = a_e \sin(\alpha)\cos\left(\frac{\theta}{2}\right) + b_e \cos(\alpha)\sin\left(\frac{\theta}{2}\right) - b_e \sin\left(\frac{\theta}{2}\right) + x_c \tag{8}$$

$$y_e = a_e \sin(\alpha)\sin\left(\frac{\theta}{2}\right) - b_e \cos(\alpha)\cos\left(\frac{\theta}{2}\right) + b_e \cos\left(\frac{\theta}{2}\right) + y_c. \tag{9}$$

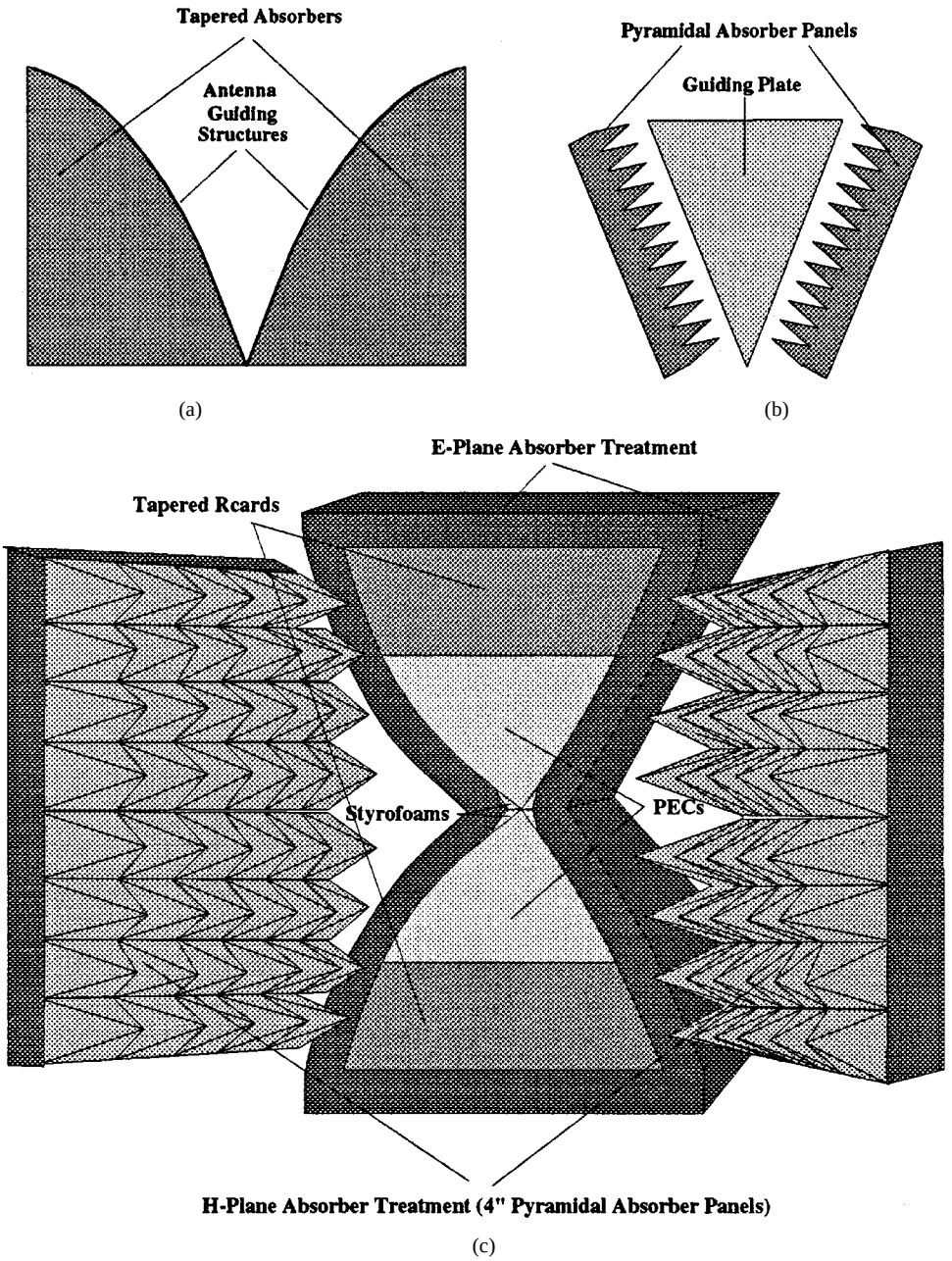

Fig. 3. (a) E-plane absorber treatment, (b) H-plane absorber treatment, and (c) simplified drawing of an Rcard SBH antenna after adding E- and H-plane absorber treatment.

Note that a and b are the ellipse major and minor axis lengths, respectively, and α is the ellipse sweeping angle, which starts at 0° and ends at α_s.

The feeding structure discussed in the previous section is smoothly connected to the Vivaldi section of the guiding structure to properly guide the slotline mode into the bowtie guiding plates. This connection is the same as the conducting SBH antenna developed by Lai *et al.* [3]. The major difference is that the large conducting rolled edges in the original conducting SBH antenna have been replaced by much smaller tapered Rcard rolled edges in the new "Rcard SBH" version, as shown in Fig. 2. Much like the original SBH antenna, the E- and H-plane patterns can be designed separately. According to given specifications, one normally focuses on the E-plane design using numerical analysis and then properly chooses the bowtie plate angle to satisfy the H-plane specification [11].

The analytical tool to design the guiding structure is the TECYL code developed by Richmond [12]. This code only models the surface contour in the E-plane cut based on the assumption that the impact on the E-plane pattern due to edge waves along the finite width plate and Rcard can be neglected. Since this approach reduces the three-dimensional complexity of the SBH antenna geometry to a two-dimensional problem, the E-plane radiation pattern can be calculated very efficiently in terms of computational memory and time. Note that the above assumption is generally not valid in that the edge waves are normally significant enough that they can distort the radiation patterns. However, it will be shown in later

sections that absorber materials can be employed to reduce these undesired mechanisms so that the E-plane radiation pattern can be accurately predicted by the TECYL code.

In practice, the Rcard SBH antenna is designed through an optimization process (see Section V) to achieve the best possible performance. However, to be able to properly guide the optimization routine, one needs to understand the impact of the various design parameters on the resulting radiation patterns. The total parameters associated with an Rcard SBH antenna design can be classified into three categories (refer to Fig. 2):

1) parameters for VSWR: Vivaldi length ($x_b - x_a$) and flare angle (θ);
2) parameters for antenna geometry: flare angle (θ), linear section length ($x_c - x_b$), and rolled-edge section parameters (a, b, α_s, $nblend$);
3) parameters for resistive sheets: [R_1, R_2, Rcard length(Rcardln)].

Note that the bowtie flare angle (θ) is listed in the first two categories in that it is a common parameter, which has an impact on both the VSWR and radiation patterns. Even though there are 11 antenna design parameters listed above, only seven parameters are independent and should be considered in the design process. They are the bowtie flare angle (θ), the PEC length in the guiding structure ($PEC\ln$), the maximum sheet resistance ($R_{\max}$), the rolled-edge blending function type ($nblend$), the rolled edge ellipse major (a) and minor (b) axes, and the maximum sweep angle (α_s). These parameters should be determined such that the diffracted fields due to the truncation of the antenna structure are minimized. Based on the TECYL code analysis of the E-plane pattern, some conclusions related to the above design parameters are listed below.

TABLE I
DESIGN PARAMETERS OF THE RCARD SBH ANTENNA

Feeding Structure Parameters	
Microstrip Line Width (W_m)	80 mil
Slot Line Width (W_s)	2 mil
Dielectric Thickness (h)	30 mil
Cladding Thickness (t)	0.7 mil
Relative Dielectric Constant (ϵ_r)	2.94
Vivaldi Section Parameters	
Exponential Factor (A)	0.44
Section Length ($X_b - Xa$)	2.1 cm
Linear Section Parameters	
Section Length ($X_c - Xb$)	1.9 cm
Bowtie Flare Angle (θ)	60°
Rolled Edge Section Parameters	
Major Axis Length (a)	28 cm
Minor Axis Length (b)	14 cm
Maximum Sweep Angle (α_s)	60°
Blending Function	Linear Blending
Bowtie Plate Parameters	
Bowtie Plate Angle	(50°)
PEC Length ($PECln$)	18 cm
Rcard Length ($Rcardln$)	11.5 cm
Rcard Parameters	
Resistive Distribution	Exponential Function
Lowest Sheet Resistance (R_{min})	3Ω/□
Highest Sheet Resistance (R_{max})	3000Ω/□

A. Flare Angle (θ)

The flare angle is directly related to the antenna beamwidth. If the flare angle is small, all the rays from the throat of the antenna reach the aperture with a small phase difference. In such cases, the antenna pattern, which can be evaluated by the Fourier transform of the aperture current, is narrower when the flare angle (or equivalent aperture size) is smaller provided the antenna is long enough. If the flare angle is large, the antenna mainbeam is dictated by the geometrical optics field radiated directly from the antenna throat or phase center. In such a case, a wider flare angle causes a wider antenna beamwidth. Thus, the E-plane beamwidth monotonically decreases as the flare angle decreases provided the other parameters are chosen properly.

B. Rolled-Edge Geometry (a, b, α_s, and $nblend$)

The rolled-edge geometry is determined by the major (a) and minor (b) axes, maximum sweep angle (α_s), and blending function. Basically, if the curvature in this section increases, the transition region of diffraction fields (creeping waves) is wider, which results in a wider E-plane beamwidth. This observation implies that based on the same (a, b, $\alpha_{\max}$), using a cosine blending function will yield the narrowest beamwidth, while the elliptical curvature without any blending will result in the widest beamwidth [11]. Obviously, for the same curvature, if α_s is increased, edge diffractions will be reduced, which results in lower side and backlobes.

C. Maximum Sheet Resistance ($R_{\max}$)

It has been found [11] that an exponential Rcard taper performs best and that the maximum resistivity $R_{\max}$ is related to the Rcard length. If the available Rcard length is not long, the optimal $R_{\max}$ to minimize the backlobe will not be as large a value. Note that for ultrawide-bandwidth applications, the Rcard length is determined by the wavelength ($\lambda_{\max}$) of the lowest operating frequency. In most cases, the Rcard length is at least one $\lambda_{\max}$, which results in $R_{\max}$ typically in the 1000 ($\Omega/\square$) range [11].

D. PEC Length (PEC$\ln$) and Rcard Length (Rcard$\ln$)

One should notice these two parameters are dependent on each other in that once the antenna geometry and PEC$\ln$ are specified, the Rcard length (Rcard$\ln$) is determined accordingly.

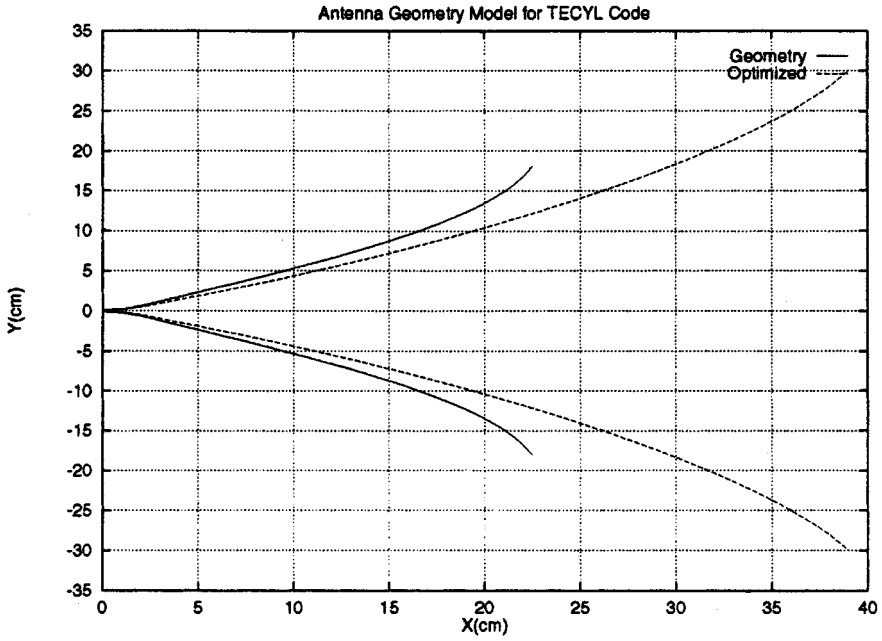

Fig. 4. Numerical models of Rcard SBH guiding structure. Optimized and nonoptimized geometries are compared.

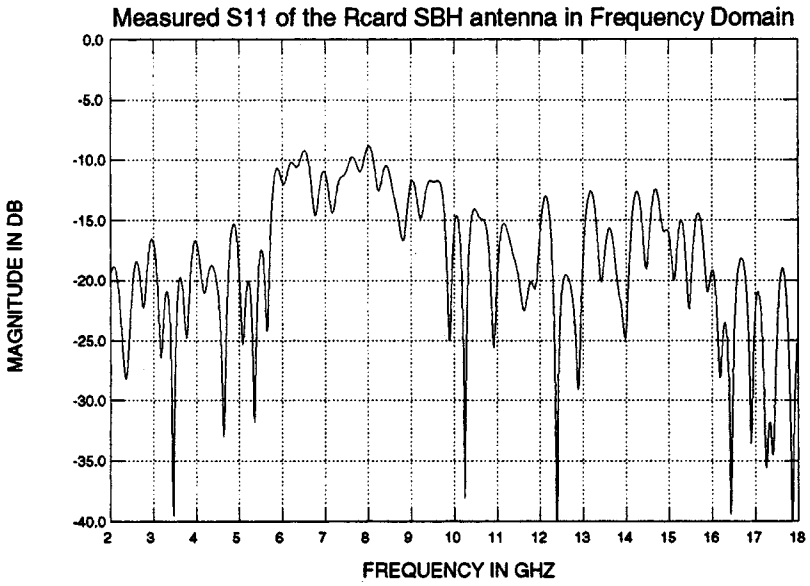

Fig. 5. Measured S11 of a typical Rcard SBH antenna.

The ratio of Rcardln to PECln in the guiding structure has a significant impact on the overall antenna pattern. It has been found [11] that a longer Rcardln (or shorter PECln) can reduce the diffracted fields and stabilize the beamwidth variation versus frequency. However, this does not imply that one can increase the Rcard length without limit because the geometrical optics fields will be attenuated if Rcardln is too long, which then results in a narrower beamwidth.

IV. Absorber Treatment

Proper absorber treatment is required in the antenna construction to reduce the stray signals due to the open structure of the SBH antenna [3], [11]. It has been found that the absorber treatments used in the E- and H-planes are not the same due to their different boundary conditions. In the E-plane, the E field is guided by the top and bottom guiding plates. However, because of the sharp plate edges, as has been found by Lai [3], edge waves are created, which travel along the edges and eventually radiate. Therefore, the absorber treatment in the E-plane should be applied right behind the guiding structure, as shown in Fig. 3(a), to attenuate these undesired mechanisms.

For the H-plane, the absorber should be applied to the side walls of the H-plane cut as shown in Fig. 3(b) to attenuate the spillover due to the fringing fields associated with the guiding plates. It is obvious that this absorber should possess a low reflection nature such that the fringing fields are not significantly

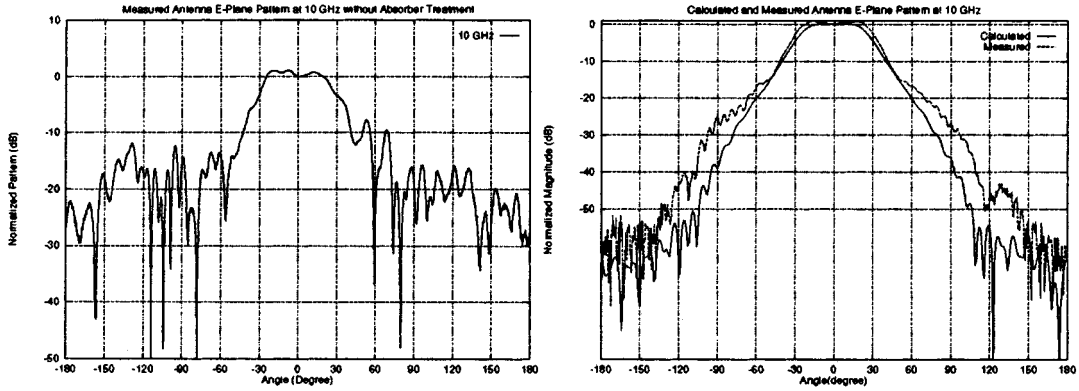

(a) (b)

Fig. 6. Measured E-plane radiation patterns at 10 GHz (a) without absorber treatment and (b) with absorber treatment.

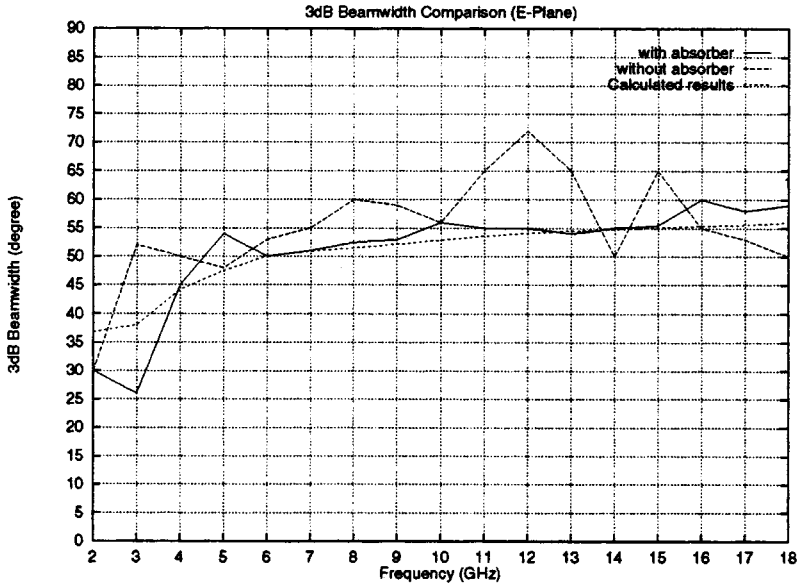

Fig. 7. Comparison of E-plane 3-dB beamwidths associated with the calculated and measured results, with and without absorber treatment.

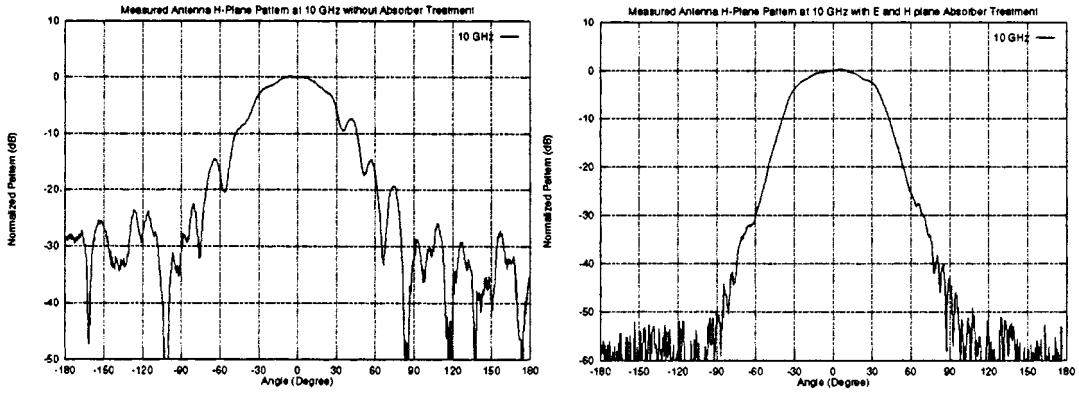

(a) (b)

Fig. 8. Measured H-plane radiation patterns at 10 GHz (a) without absorber treatment and (b) with absorber treatment.

attenuated inside the absorber. It has been found [11] that a pyramidal absorber is an ideal choice for this application based on two reasons. First, its reflection coefficient is polarization independent for normal incidence. Thus, it can be placed in the fringing field without considering the incident polarization. Secondly, it has a smoother air to absorber transition so that a lower reflection coefficient level can be obtained. The performance of the E- and H-plane absorber treatment is demonstrated by the measured results in the next section.

V. Design Examples

In this section, two design examples of the Rcard SBH antenna are presented. In the first example, an empirically de-

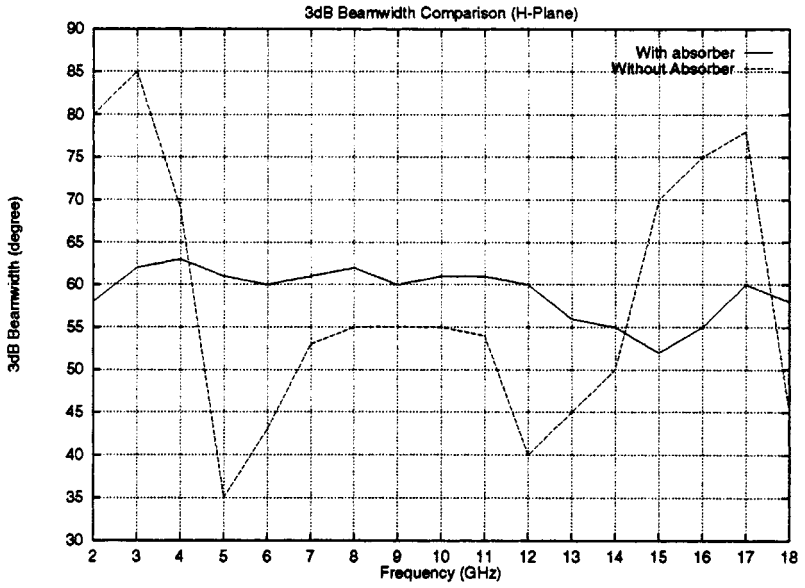

Fig. 9. Comparison of the measured H-plane 3-dB beamwidths with and without absorber treatment.

signed antenna is presented to verify the design concept based on its measured pattern and VSWR performance. In the second example, an optimization routine based on the concept of the genetic algorithm is introduced to demonstrate the optimization process associated with the Rcard SBH antenna design.

A. Design of an Rcard SBH Antenna

The goal of this design is to develop an Rcard SBH antenna with constant beamwidth across the 2–18 GHz frequency band that has similar E- and H-plane patterns with a plateau mainbeam. The design parameters are listed in Table I, and the antenna geometry for the E-plane numerical modeling is shown in Fig. 4. A typical antenna VSWR (S11), which was measured using an HP-8510 network analyzer, is shown in Fig. 5. This antenna was built by Rockwell International and measured in the OSU-ESL compact range. The measured E-plane radiation pattern at 10 GHz before the absorber treatment was added is shown on the left side of Fig. 6. This result illustrates significant mainbeam ripple and high side and back lobes, which are due to the stray signals associated with the open antenna structure. After applying the E-plane absorber treatment, the measured result at the same frequency (10 GHz) is shown on the right side of Fig. 6. The calculated radiation pattern is also shown for comparison. The E-plane 3-dB beamwidths with and without the absorber treatment are compared with the calculated result as shown in Fig. 7. It is obvious that the absorber treatment has greatly improved the antenna performance by reducing the undesired mechanisms. The remaining ripple in the mainbeam is mostly due to construction defects around the antenna throat of this prototype model. This argument will be verified by the next design example. Nevertheless, the measured E-plane patterns, after the absorber treatment had been added, were found to be in good agreement with the calculated results, which verifies the design concept and numerical modeling.

Next, the H-plane radiation patterns are investigated. Fig. 8(a) shows the H-plane measured result at 10 GHz without the H-plane absorber treatment. One can observe that the stray signals have an impact on both the E- and H-plane patterns. After the absorber treatment was added, as shown in Fig. 3(c), the measured H-plane pattern at 10 GHz, as shown in Fig. 8(b), was obtained. Significant improvement can be readily observed in this figure. In addition, the measured H-plane 3-dB beamwidths with and without absorber treatment are shown in Fig. 9. After adding the complete absorber treatment, one can easily observe that the E- and H-plane radiation patterns are very similar and the 3-dB beamwidths are reasonably stable (about 60°) from 2 to 18 GHz, but not as stable as desired.

TABLE II
SOLUTION DOMAIN OF THE ANTENNA DESIGN PARAMETERS FOR THE GA OPTIMIZATION PROCESS

Parameter	Lower Bound	Upper Bound	Quantization Level
Flare Angle	43.	51.	32
PEC Length	20.	30.	32
Major Axis (a)	46.	60.	32
Minor Axis (b)	11.	25.	32
α_{max}	54.	70.	32

TABLE III
OPTIMAL PARAMETER VALUES AFTER THE GENETIC OPTIMIZATION PROCESS

Parameter	Optimal Value
Flare Angle	49.258
PEC Length	25.806
Major Axis (a)	48.710
Minor Axis (b)	20.032
α_{max}	63.806

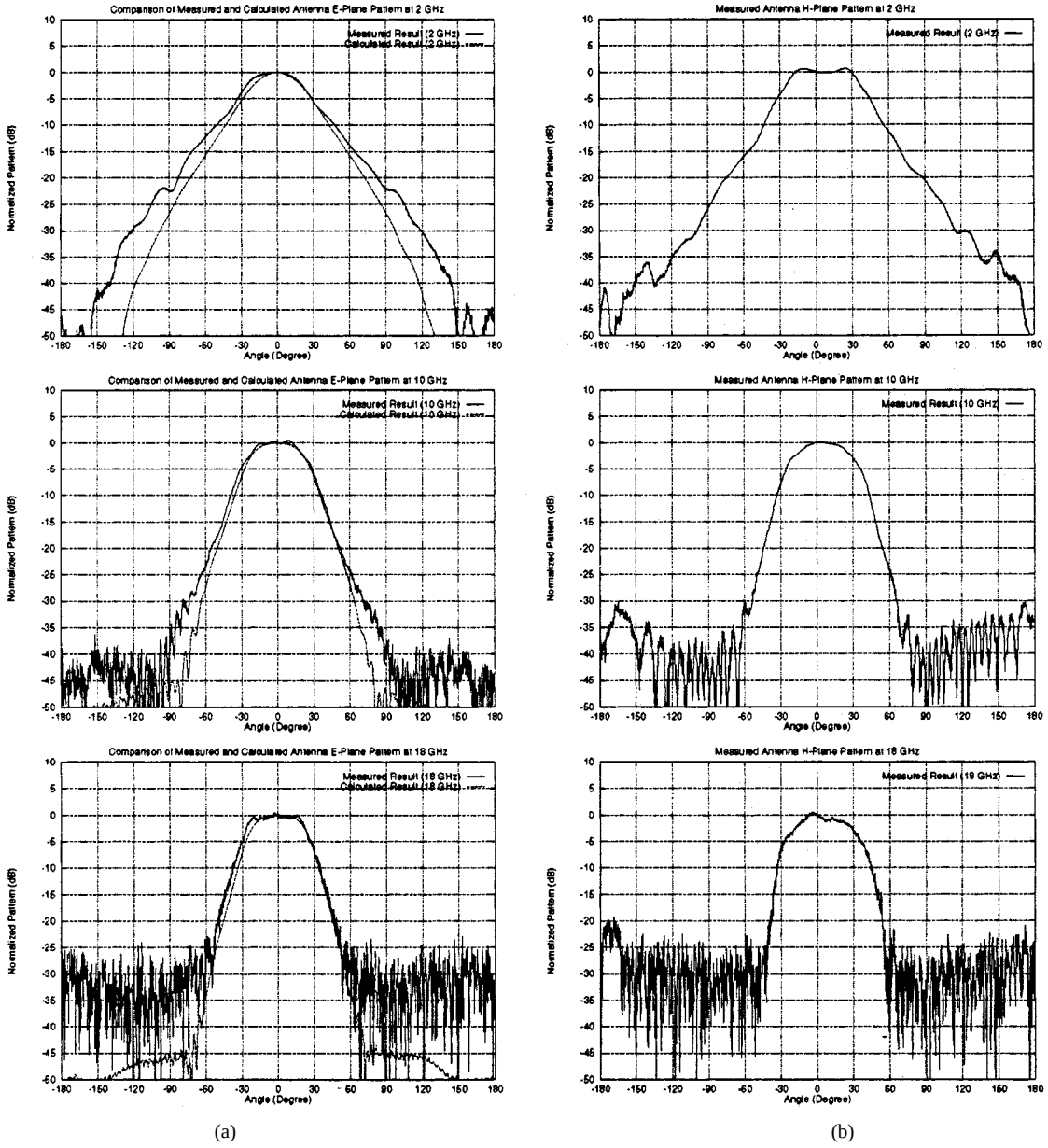

(a) (b)

Fig. 10. Measured (a) E-plane and (b) H-plane radiation patterns at 2, 10, and 18 GHz associated with the optimized Rcard SBH antenna.

B. Genetic Optimization Design

Recall that the previous antenna was empirically designed, and that the 3-dB beamwidths were not as stable versus frequency as desired. In this section, an optimization process based on the concept of the genetic algorithm (GA) [10] is introduced to improve the beamwidth stability performance. The antenna specification associated with this design example should have a constant 47° 3-dB beamwidth from 2 to 18 GHz in both the E- and H-planes. No blending function is employed in this design to reduce the ripple in the mainbeam. Also, the highest sheet resistance ($R_{\max}$) was chosen to be 1000 ($\Omega/\square$) so that available Rcards could be used. Therefore, the optimization routine focuses on the antenna geometry design, which, according to Section III, involves five design parameters: the flare angle (θ), PEC length ($PEC\ \ln$), ellipse major and minor axes (a, b) and maximum sweep angle ($\alpha_{\max}$) in the rolled-edge section. The cost function was defined to be the 3-dB beamwidth of the radiation pattern calculated through the TECYL code based on the five input parameters.

Table II illustrates the solution domain of these five parameters. These parameter bounds were determined based on the physical insight provided in Section III. For example, it is known that the flare angle θ is directly related to the 3-dB beamwidth. To obtain a constant 3-dB beamwidth of 47°, it is obvious that the flare angle cannot deviate too much from 47°. In this design, the solution domain of the flare angle was chosen between 43° and 51°, which is centered at 47° with a 4° offset. To simplify the GA process, each parameter was quantized and encoded in a binary string. Due to the solution domain being properly defined, only 16 populations were needed in this process, and a 2% mutation was employed. After 25 iterations, the process converged, and the optimal values associated with the above design parameters are listed in Table III.

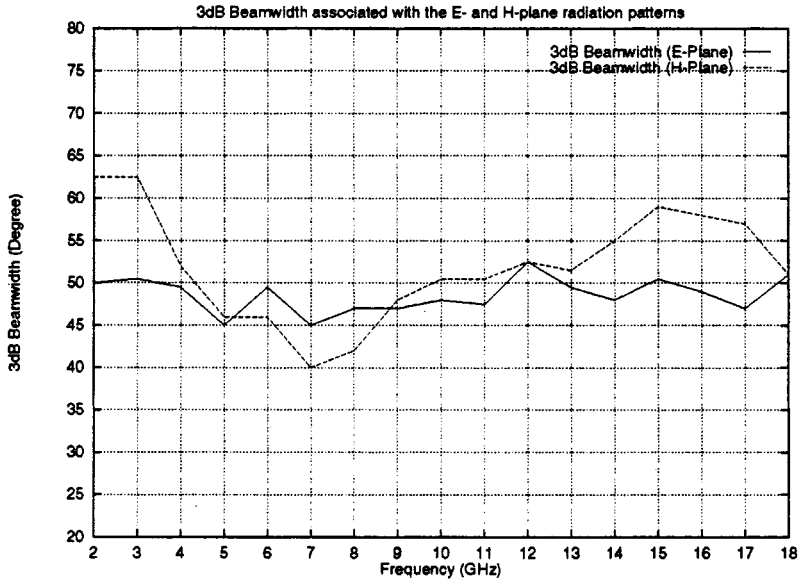

Fig. 11. Measured 3-dB beamwidths versus frequency associated with the E- and H-plane radiation patterns.

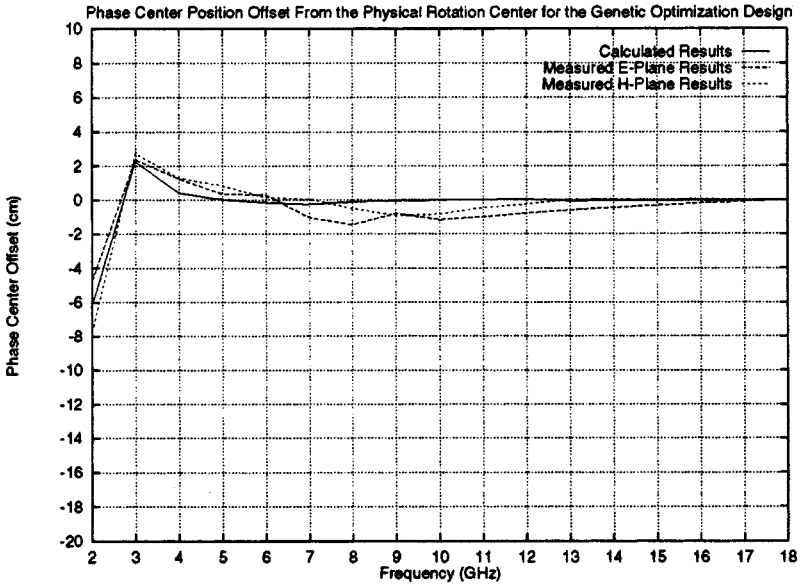

Fig. 12. Phase center offset versus frequency associated with the E- and H-plane radiation patterns.

The antenna geometry based on the optimized parameters is also shown in Fig. 4. The measured E- and H-plane patterns at 2, 10, and 18 GHz are shown in Fig. 10. Note that the calculated E-plane patterns are also shown as a reference result. The measured 3- dB beamwidths in both planes are plotted in Fig. 11. One can observe that excellent agreement is obtained between the measured and calculated E-plane patterns associated with this optimized antenna. The average E-plane 3-dB bandwidth is about 49°, which is very close to the design specification (47°). The mainbeam ripple is much smaller than the previous design due to improved construction techniques. For the H-plane pattern, one can observe that well-defined H-plane mainbeam patterns have also been obtained from 2 to 18 GHz. However, more significant beamwidth variations, especially in the intermediate frequencies, can be seen in this antenna than the first design. A possible reason to account for this phenomenon is that the antenna geometry in this design was constructed without any blending function, while the first antenna employed a linear blending function in its rolled-edge geometry. In other words, this antenna has more curvature in the guiding structure, which tends to cause more fringing field variations versus frequency in the H-plane results.

It is instructive to investigate the phase center variation in terms of frequency for this optimized antenna. Fig. 12 shows the antenna phase center variation from 2 to 18 GHz based on the measured E- and H-plane radiation patterns. The phase center variation based on the calculated results is also shown as a reference. Note that the phase center position was estimated by adjusting the phase term associated with the radiated field in order to obtain a uniform phase variation across the mainbeam region. One can observe that in general, the antenna phase center is very stable from 3 to 18 GHz. The phase center is slightly closer to the

antenna aperture at 2 GHz, which is due to the diffracted fields associated with the antenna termination still being significant at the lowest operating frequency for this design. Nevertheless, based on the above measured results, one can clearly see that the concept of using the genetic algorithm to optimally design this new Rcard SBH antenna has been verified.

VI. Summary and Conclusion

An ultrawide-bandwidth low-RCS horn antenna, namely, the Rcard SBH antenna, has been presented. This antenna is a modified version of the original conducting SBH antenna by introducing tapered Rcard materials in the antenna guiding structures to replace the original large conducting rolled-edge terminations. Due to the smaller antenna geometry and the Rcard's partially transparent nature with respect to electromagnetic fields, this new SBH antenna can achieve similar performance to the original conducting SBH antenna and, at the same time, possess a smaller antenna RCS. However, to achieve the desired features, this antenna requires absorber treatment in both the E- and H-planes.

An optimization routine based on the concept of the genetic algorithm has also been discussed in this paper to optimize the antenna performance. Through the optimization process, Rcard SBH antennas have been designed that possess constant E- and H-plane 3-dB beamwidths and stable phase centers over an ultrawide bandwidth. As a result, this new antenna should be very useful for a wide variety of applications.

References

[1] J. L. Kerr, "Short axial length broad-band horns," *IEEE Trans. Antennas Propagat.*, vol. AP-21, pp. 710–714, Sept. 1973.

[2] EM Systems, Inc., "Performance characteristics of model A6100 dual-polarized quadridged horn," EM Systems, Inc., Oct. 1984.

[3] K. Y. A. Lai, A. L. Sinopoli, and W. D. Burnside, "A novel antenna for ultrawide-band applications," *IEEE Trans. Antennas Propagat.*, vol. 40, pp. 755–760, July 1992.

[4] B. Schiek and J. Kohler, "An improved microstrip-to-microslot transition," *IEEE Trans. Microwave Theory Tech.*, vol. MTT-24, pp. 231–233, Apr. 1976.

[5] P. J. Gibson, "The Vivaldi aerial," in *Proc. 9th Eur. Microwave Conf.*, Sept. 1979, pp. 101–105.

[6] I. J. Gupta, K. P. Ericksen, and W. D. Burnside, "A method to design blended rolled edges for compact range reflectors," *IEEE Trans. Antennas Propagat.*, vol. 38, pp. 853–861, June 1990.

[7] A. L. Sinopoli, "A slotline/bowtie hybrid antenna for use as a compact range feed," M.S. thesis, Dept. Elect. Eng., Ohio State Univ., Columbus, 1992.

[8] W. H. Darden IV, "The design of ultra-wide-band antennas with narrow beamwidths," M.Sc. thesis, Dept. Elect. Eng., Ohio State Univ., Columbus, 1993.

[9] J. H. Richmond, "Propagation of surface waves on a thin resistive sheet or a coated substrate," *Radio Sci.*, vol. 22, pp. 825–831, Sept./Oct. 1987.

[10] D. E. Goldberg, *Genetic Algorithm*. Reading, MA: Addison-Wesley, 1989.

[11] L.-C. T. Chang, "Constant beamwidth ultrawide bandwidth linearly and dual polarized antenna design," Ph.D. dissertation, Dept. Elect. Eng., ElectroSci. Lab., Ohio State Univ., Columbus, 1996.

[12] J. H. Richmond, "An integral-equation solution for TE radiation and scattering from conducting cylinders," ElectroSci. Lab., Ohio State Univ., Columbus, Rep. 2902-7, Mar. 1972.

Li-Chung T. Chang was born in Taipei, Taiwan, R.O.C, in 1966. He received the B.S. degree in electrical engineering from National Chiao-Tung University, Hsinchu-Chu, Taiwan, in 1988 and the M.S. and Ph.D. degrees in electrical engineering from The Ohio State University, Columbus, in 1993 and 1996, respectively.

From 1988 to 1990, he was with the Unified Military Communications Headquarters, Taipei, as a Communications Instructor. During his graduate studies, he was a Graduate Research Associate at the ElectroScience Laboratory, The Ohio State University. Since January 1997, he has been with Lucent Technologies, Whippany, NJ.

Walter D. Burnside (S'69–M'72–SM'82–F'85) was born in Youngstown, OH, on April 19, 1942. He received the B.S.E. and M.S. degrees in 1968 and the Ph.D. degree in 1972, all in electrical engineering, from The Ohio State University, Columbus.

Since 1966, he has been with the ElectroScience Laboratory, Department of Electrical Engineering, The Ohio State University. He is currently a Full Professor with the Department of Electrical Engineering and Director of the ElectroScience Laboratory. His main interests are in applications of wedge diffraction, the geometrical theory of diffraction, broad-band antennas, airborne antenna analysis, hybrid solutions, and various high-frequency scattering solutions. More recently, he has been working on state-of-the-art designs for scattering and antenna measurement facilities.

Dr. Burnside has won several IEEE Best Paper Awards, the Distinguished Achievement Award from the Antenna Measurement Techniques Association, a Distinguished Scholar Award from The Ohio State University, and the Distinguished Public Service Medal from NASA Headquarters. More recently, he received an Honorary Ph.D. degree from the University of Pretoria, South Africa. He was formerly an Associate Editor of the IEEE Transactions on Antennas and Propagation.